Detection of motion artifact patterns in photoplethysmographic signals based on time and period domain analysis

2014 Physiol. Meas. 35 2369

(http://iopscience.iop.org/0967-3334/35/12/2369)

IOP Publishing | Institute of Physics and Engineering in Medicine Physiological Measurement

Physiol. Meas. **35** (2014) 2369–2388 doi:10.1088/0967-3334/35/12/2369

Detection of motion artifact patterns in photoplethysmographic signals based on time and period domain analysis

R Couceiro[1], P Carvalho[1], R P Paiva[1], J Henriques[1] and J Muehlsteff[2]

[1] Center for Informatics and Systems of the University of Coimbra, Polo II, 3030-290 Coimbra, Portugal
[2] Philips Research Laboratories Europe, HTC, 5656AE Eindhoven, The Netherlands

E-mail: rcouceir@dei.uc.pt

Received 26 May 2014
Accepted for publication 5 August 2014
Published 12 November 2014

Abstract

The presence of motion artifacts in photoplethysmographic (PPG) signals is one of the major obstacles in the extraction of reliable cardiovascular parameters in continuous monitoring applications. In the current paper we present an algorithm for motion artifact detection based on the analysis of the variations in the time and the period domain characteristics of the PPG signal. The extracted features are ranked using a normalized mutual information feature selection algorithm and the best features are used in a support vector machine classification model to distinguish between clean and corrupted sections of the PPG signal. The proposed method has been tested in healthy and cardiovascular diseased volunteers, considering 11 different motion artifact sources. The results achieved by the current algorithm (sensitivity—SE: 84.3%, specificity—SP: 91.5% and accuracy—ACC: 88.5%) show that the current methodology is able to identify both corrupted and clean PPG sections with high accuracy in both healthy (ACC: 87.5%) and cardiovascular diseases (ACC: 89.5%) context.

Keywords: photoplethysmography, motion artifacts; period domain analysis, time domain analysis, feature extraction, feature selection, support vector machine

(Some figures may appear in colour only in the online journal)

1. Introduction

Photoplethysmography (PPG) is a non-invasive, low cost tool to continuously monitor blood volume changes in tissue as a function of time. One of the major advances of the PPG-based technology in clinical environments is the pulse oximeter, which has been accepted by the International Standards Organization (ISO) and the European Committee for Standardization as the standard non-invasive measure of oxygen saturation level since 1987 (Shang *et al* 2007). Motivated by unmet needs in low cost, unobtrusive and portable techniques in personal-Health (p-Health), the PPG technique has been object of extensive research in the later decades. Due to technological advances in the field of opto-electronics, clinical instrumentation and digital signal processing, the PPG technique achieved a broader spectrum of potential applications, ranging from the field of clinical physiological monitoring to the vascular assessment, and autonomic function evaluation (Allen 2007). Moreover, this technique has been widely applied in many clinical areas such as anesthesia, surgical recovery and critical care (Allen 2007).

However, the quality of the PPG signals can be easily influenced by properties of the light-emitting diode and photodetector, as well as the pressure exerted on the PPG probe, which may affect the morphology of the PPG waveform (Reisner *et al* 2008). Moreover, the ambient light at the photodetector, poor blood perfusion of the peripheral tissues and motion artifacts (Sukor *et al* 2011) are also common sources of errors. In uncontrolled environments such as home care settings, these potential error sources are more frequent and can become a serious obstacle to the reliable use of PPG derived parameters, especially in continuous monitoring applications. Therefore, it is important to provide signal quality or trust metric that provides the subsequent analysis algorithms with a level of trust in the derived parameters, which reduces the false alarms, allows identifying inaccurate readings and finally increases patient safety.

Although the recent technological advances allowed the minimization of some of these limitations, motion artifact detection and suppression is still a major challenge (Allen 2007, Sukor *et al* 2011) in particular without using additional sensors. Indeed, the field of motion artifact and noise suppression has been subject of intensive research in the last decade. Various approaches have been investigated, where the clean PPG signal is recovered or reconstructed from the corrupted one. A common approach in this field is to use adaptive filtering techniques (Graybeal and Petterson 2004, Lee *et al* 2004, Foo and Wilson 2006, Kunchon *et al* 2009) to reduce noise and motion artifacts. In these approaches, an adaptive filter (e.g. Least Mean Square adaptive filter) is applied as a joint process estimator to cancel noise and motion artifacts and consequently retrieve a clean PPG signal. However, some studies indicate that these techniques introduce phase shifts in the PPG signal, which may compromise its subsequent interpretation (Foo 2006). Additionally, similar findings have been shown for wavelet based transformation techniques.

Another common approach is to use accelerometers as a reference noise signal to cancel out motion artifacts in PPG signals (Gibbs and Asada 2005, Han *et al* 2007, Kim *et al* 2007, Wood and Asada 2007). However, these methods present major drawbacks. Here, an accelerometer needs to be coupled to the PPG sensor in order to retrieve the noise reference and synchronisation of both signals, which makes this approach hardly suitable for current equipment in clinical settings. Additionally, there is not a direct correlation between movements (acceleration data) and motion artifacts in PPG (Yousefi *et al* 2012).

Other authors opted to use time-frequency analysis (Lee and Zhang 2003, Yan *et al* 2005, Reddy *et al* 2008, Raghuram *et al* 2012) and source separation techniques (Kim and Yoo 2006) to recover the clean PPG signal. Reddy *et al* (Reddy and Kumar 2007) proposed a motion artifact reduction method based on singular value decomposition. Later in (Reddy *et al* 2008), the same author applied a beat-by-beat Fourier series analysis to reconstruct a

clean PPG signal. Yan *et al* (2005) applied a smoothed pseudo Wigner–Ville distribution for reduction of motion artifacts. Raghuram *et al* (2012) proposed the use of an empirical mode decomposition technique combined with the Hilbert–Huang transform to reconstruct clean PPG section from the corrupted PPG signal. Kim *et al* (Kim and Yoo 2006) proposed the combination of a block interleaving and low pass filtering technique approach with an Independent Component Analysis technique to separate the PPG from motion artifacts. These techniques assume that underlying a corrupted PPG signal there is a clean/uncorrupted reference capable of being retrieved, which is not often possible. Additionally, the distortion induced by the reconstruction of a clean PPG signal can significantly bias the extracted measurements (e.g. left ventricular ejection time—LVET) and induce subsequent wrong diagnosis.

In many applications (hospital as well as home monitoring), an alternative to noise reduction is the robust detection of PPG signal sections corrupted by noise and motion artifacts and exclude them from the subsequent analysis. Techniques such as morphological analysis (Sukor *et al* 2011) and higher-order statistical analysis (Krishnan *et al* 2008) have been proposed in this research field. Sukor *et al* (2011) proposed an algorithm based on the analysis of several morphological characteristics of the PPG pulses to distinguish bad quality pulses from good ones. The author reports that the proposed methodology is able to identify motion artifacts with an accuracy of 83%. Krishnan *et al* (2008) used a sensor fusion approach combining high order statistical features from the time and frequency domain to discriminate corrupted PPG sections. The proposed methodology was able to detect motion artifacts with a probability of 91% and a false alarm probability of 0.06%.

Despite the good results presented in (Sukor *et al* 2011), we believe that motion artifact detection performance can still be increased. It is our goal not only to evaluate the changes in the morphological characteristics of the PPG signal, but also to utilize the idea that clean and corrupted PPG sections have different period characteristics. It is still unknown which time/period characteristics best distinguish clean and corrupted PPG sections and it is expected that these characteristics depend on the target population in clinical practice. Therefore, a study regarding the evaluation of the best features in the time and period domain for artifact discrimination and their application in both healthy and cardiovascular diseased (CVD) populations has yet to be developed.

In this paper, we present a motion artifact detection methodology, which is based only on the analysis of the time and period domain characteristics of the PPG signal from 8 healthy volunteers and 7 CVD patients. In the time domain analysis we evaluate the changes in the main morphological characteristics of the PPG beats. In the period domain analysis, the period characteristics of the PPG signal are assessed and compared using a sliding window approach. Several features are extracted, and the Normalized Mutual Information Feature Selection (NMIFS) algorithm (Estevez *et al* 2009) is used to select the most relevant and least redundant ones. The most discriminative features are used as inputs to a Support Vector Machine (SVM) classification model.

The paper is organized as follows: the proposed methodology is introduced in section 2. The results and respective discussion are presented in section 3. Finally, the conclusions are summarized in section 4.

2. Methods

The proposed methodology for the detection of motion artifacts consists of the following stages (see figure 1): (a) pre-processing and baseline removal; (b) segmentation; (c) feature extraction; (d) feature selection and (e) classification.

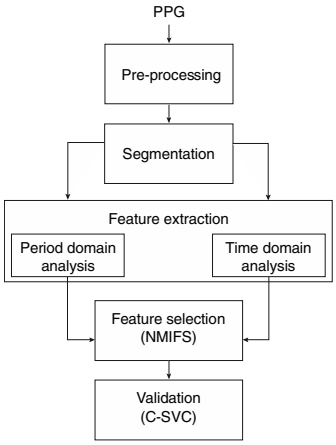

Figure 1. Scheme of the proposed motion artifacts' detection methodology.

2.1. Pre-processing

The goal of the pre-processing stage is to remove the frequency components that do not represent the fundamental features of the PPG signal. Based on the algorithm proposed in (Chan *et al* 2007), the high frequency components which are not physiologically related to the PPG waveform were removed using a low-pass Butterworth filter with a 18 Hz cut-off frequency and a 2 s window moving average filter is applied to derive an approximation of the PPG signal baseline, which is subtracted from the original PPG signal.

2.2. Segmentation

The morphology of the PPG pulse is a result of a complex interaction between the left ventricle and the systemic circulation. It is composed of an early main pulse created by the ventricular contraction and various additional pulses caused by pressure pulse reflections in the central arterial tree to the peripheral vasculature. As the main pulse (P1—illustrated in figure 2) arrives at the first reflection site, which is, the junction between the thoracic and abdominal aorta, there is a significant decrease in the artery diameter along with the change in its elasticity causing the main pulse to be reflected. The main pulse continues to travel downwards and reaches the second reflection site, which arises from the juncture between abdominal aorta and common iliac arteries (Baruch *et al* 2011). These reflection sites are commonly known as the renal and iliac reflections sites and give rise to the second (commonly known as second systolic peak) and third reflection waves (P2 and P3, respectively—illustrated in figure 2). Additionally, there are also other minor reflections and re-reflections in the systemic structure that give rise to smaller reflection waves.

Commonly, in healthy individuals, these reflection waves occur during early diastole and a dicrotic notch can be observed between the first and second PPG peaks. Contrarily, in elder individuals and/or individuals with cardiovascular diseases, the vascular properties may lead to a significant increase of the pulse wave velocity up to a factor of three (e.g. due to arterial stiffening), leading to the occurrence of the reflected waves during late systole and preventing the distinction between direct and reflected waves.

The main objective of the segmentation step is to detect the characteristic points correspondent to the onset and offset of the PPG pulses and allowing the posterior extraction of

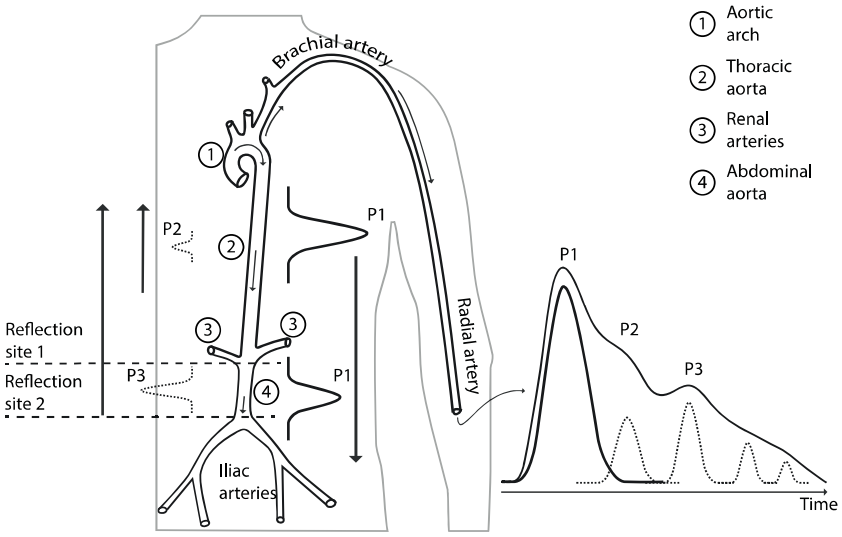

Figure 2. Morphology and origin of the PPG pulse. On the left, a PPG pulse and correspondent forward and reflected waves are presented. On the right, a sketch of the arterial system from the aorta/arm to the iliac arteries (Baruch *et al* 2011).

their morphological characteristics. We determine the characteristic points by analyzing the derivatives of the PPG signal. The physiological basis of this approach was firstly reported (Cook 2001, Wisely and Cook 2001) where Cook observed the similarity between the arterial flow waveform and the first derivative of the PPG waveform. Therefore, the point in time where the PPG first derivative is the steepest corresponds to the onset of the pulse, which can be determined as a maximum in the PPG third derivative.

To detect these characteristic points, the PPG signal is firstly differentiated using a five-point digital differentiator (Abramowitz and Stegun 2012) (equations (1)–(3)), resulting in first to third order derivatives (d1_ppg, d2_ppg and d3_ppg).

$$d1\_ppg = f'(t) = \frac{f(t-2h) - 8f(t-h) + 8f(t+h) - f(t+2h)}{12h^2} \tag{1}$$

$$d2\_ppg = f''(t) = \frac{-f(t-2h) + 16f(t-h) - 30f(t) + 16f(t+h) - f(t+2h)}{12h^2} \tag{2}$$

$$d3\_ppg = f'''(t) = \frac{-f(t-2h) + 2f(t-h) - 2f(t+h) + f(t+2h)}{2h^3} \tag{3}$$

where f is the PPG time series, t is the time index and h is the sampling time.

The 1st derivative local maxima (d1_ppg_lmax) with absolute amplitude greater than a threshold ThR are detected, where ThR is selected based on an adaptive thresholding of the d1_ppg data cumulative histogram (using a 10 s window) (Sun *et al* 2005). ThR was defined as the greater value bellow which 90% of the observations are found. Consequently, the d3_ppg local minima (d3_ppg_lmin) corresponding to the d1_ppg local maxima are also identified in order to detect the onset/offset of each PPG beat (see figure 3). These are identified as the peak with greater amplitude (d3_ppg_lmax) prior to the previously identified most relevant valley, the d3_ppg_lmax (Chan *et al* 2007).

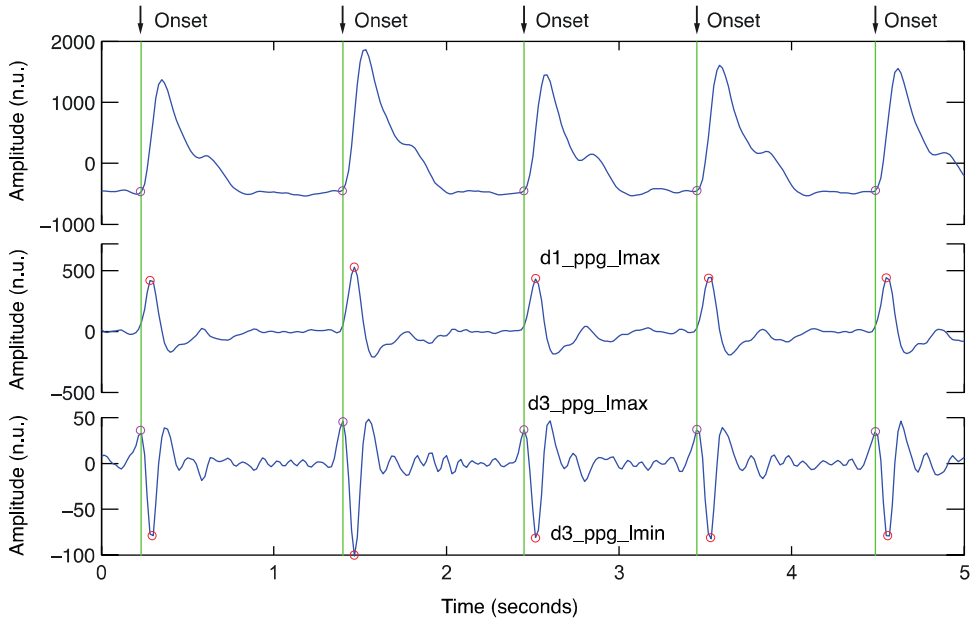

Figure 3. Plot of PPG signal derivatives (order 1–3) and representation of the detected characteristic point for the detection of the onset of each individual PPG pulse.

2.3. Feature extraction

In order to detect PPG motion artifacts it is essential to extract a set of features capable of discriminating clean from corrupted PPG sections. These features were extracted resorting on the analysis of the time and period domain analysis of the PPG. In the time domain analysis, the main goal is to capture the changes in the morphological features of the PPG pulses. In the period domain, the characteristics of principal components of the period spectrum and their relationships are evaluated.

2.3.1. Time domain analysis. In clean PPG signals, the changes on the PPG pulse morphology are mainly caused by cardiovascular changes. Contrarily, PPG signals corrupted by motion artifacts present abnormal, erratic and 'random' characteristics which can be detected from the analysis of each pulse. To assess these changes, the morphology of the PPG pulses and their relationships with the neighboring pulses are analyzed, leading to the definition of the following characteristics: (1) pulse amplitude; (2) pulse length; (3) peak distance; (4) trough depth difference; (5) peak height difference; (6) pulse skewness; and (7) pulse kurtosis. Along with the morphological characteristics proposed by Sukor *et al* (2011) (pulse amplitude, pulse length and trough depth difference), four other characteristics are introduced in the present time domain analysis of PPG signal.

As illustrated in figure 4 the pulse amplitude is defined as the difference between the pulse peak height and its preceding trough depth (pulse onset), the pulse length is the time interval between the onset of two consecutive pulses and the peak distance is the time interval between maxima of two consecutive pulses. The difference between the peak height and peak depth of two consecutive pulses was also considered. As can be observed, these characteristics change drastically in the presence of motion artifacts, showing an erratic pattern. Contrarily, clean PPG

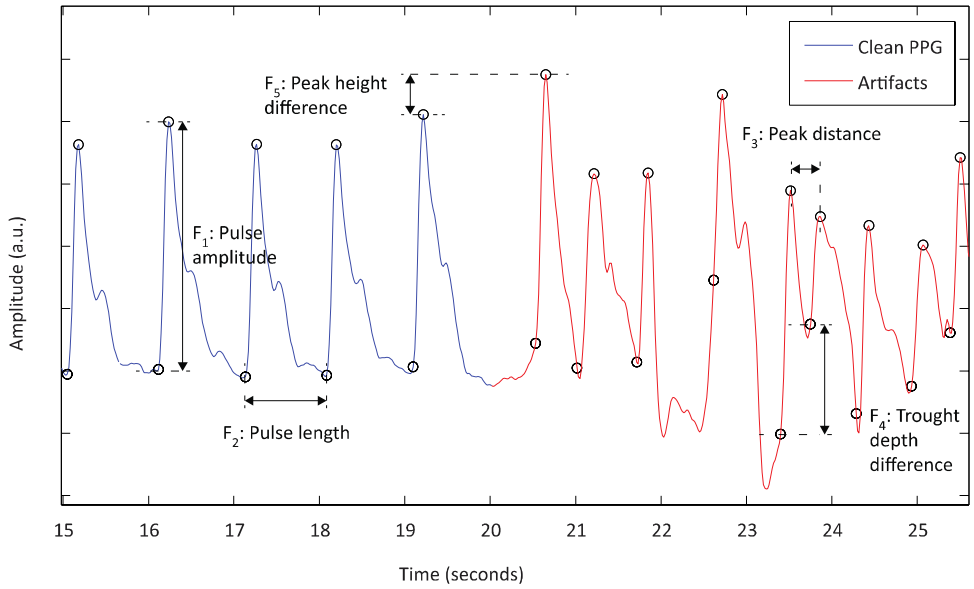

Figure 4. Plot of a PPG signal with clean and motion artifact corrupted sections. Representation of the PPG pulses morphological characteristics extracted during time domain analysis step.

sections exhibit slow variations in the aforementioned characteristics, which are a result of a variety of cardiovascular and respiratory factors (e.g. vasomotion/compliance effects, changes in venous pooling related to heart rate/cardiac output variations, blood pressure changes and respiratory modulations) (Addison *et al* 2012). For example, the PPG pulse amplitude, which is related to changes in the intrathoracic pressure during respiration (Addison *et al* 2012), exhibits slow variations in the clean PPG sections when compared to the corrupted PPG sections, where it exhibits strong and inconsistent changes between pulses.

Since the shape of the PPG pulse is highly affected by motion artifacts it is expected to see random changes in the corrupted PPG pulses symmetry and 'peakedness', which were assessed using skewness (equation (4)) and kurtosis (equation (5)).

$$Ch_6 = \frac{E\left(f_P(x) - \overline{f_P(x)}\right)^3}{\sigma^3} \tag{4}$$

$$Ch_7 = \frac{E\left(f_P(x) - \overline{f_P(x)}\right)^4}{\sigma^4} \tag{5}$$

where $f_P(x)$ is the PPG pulse, $\overline{f_P(x)}$ is the mean of $f_P(x)$, σ is the standard deviation of $f_P(x)$, and $E(t)$ represents the expected value of the quantity t.

From the analysis of various types of PPG pulses, one observed that when motion artifacts are present, the aforementioned characteristics vary significantly. Contrarily, in clean PPG signals the PPG pulses are similar and therefore there is almost no variation in its characteristics, since PPG height and regularity are related to blood volume and heart rate, respectively. These physiological properties are not expected to change abruptly between consecutive pulses. Hence, rather then evaluating the values of the proposed characteristics, as suggested

in (Sukor *et al* 2011), we aim to to capture their variations. The changes in the pulse characteristics were evaluated using equation (6), resulting in the features F_1 to F_7.

$$F_i = \Delta\,(Ch_i) = |Ch_i\,(j) - Ch_i\,(j-1)\,| \tag{6}$$

where, Ch_i is the ith characteristic and j is the pulse (section) index.

2.3.2. Period domain analysis. To assess the period characteristics of the PPG signal, the discrete-time short time Fourier transform (STFT) was applied in the period domain. Let the $[x_n, ..., x_{n+N-1}]$ be the sequence defining the section of the PPG signal under analysis. For a sampling frequency SF, the frequency 'bin' k of the N-point STFT corresponds to the frequency $f_k = k\,.\,SF\,/\,N$ Hz, that is, $s_k = 1\,/\,f_k = N\,/(k\,.\,SF)$ s$= N\,/\,k$ samples. The STFT in the period domain, i.e. PD-STFT, defined as

$$X\,(n,\ s)\ = \sum_{m=0}^{L-1} x_{n+m} w_m \mathrm{e}^{-j2\pi m/s} \tag{7}$$

is the expression for the DFT of the windowed sequence $x_{n+m}w_m$ of the kth period bin. $s = 1, 2, \ldots, N-1$ samples is the range of possible periods in the aforementioned sequence.

To choose the size of the sequences (L) and the forward step (Δn), that is related to the section overlapping ($L - \Delta n$) one must take into account: (i) the stationary of the analyzed signal section; (ii) the tradeoff between the PD-STFT period and temporal resolution; (iii) the temporal resolution needed for the subsequent analysis.

Considering the aforementioned issues, the PD-STFT was applied using a rectangular-shaped sliding window with approximately 3 times the fundamental period of the PPG signal (i.e. periods from 0 to approximately one and a half beat). The fundamental period was defined as the maximum of the period domain spectrum calculated from the first 5 s of each PPG signal. The overlap between consecutive windows was set to be approximately 85%. Thus, we assume the stationarity of the signal in the analyzed section and guarantee an appropriate trade-off frequency resolution of the computed PD-STFT. Furthermore, by choosing 85% window overlap size we ensure that the analysis output has the reasonable temporal resolution (i.e. half of a beat) necessary for further analysis and motion artifact detection. Moreover, a good tradeoff between the computational complexity of the algorithm and the acquired temporal resolution is also achieved. The fundamental period was extracted and updated based on the period analysis of small sections (5 s) of the PPG signal.

From the obtained period domain spectra characteristic features are extracted. This procedure resorts on the principle that, similarly to the morphology of the PPG signal, the PD-STFT also exhibits a regular shape representing the main features of the signal. From an analysis of the PD-STFT of various PPG classes (Dawber *et al* 1973) one observed that the PD-STFT of a clean PPG signal consists of three major spikes (P_1, P_2 and P_3) with positioned at different locations and with different widths, heights and areas (figure 5). The most relevant spike corresponds to the fundamental period of the PPG signal, i.e., the length of the cardiac cycle (beat). The remaining spikes are thought to be associated with the location and amplitude of the waves reflected from the periphery towards the aorta. Based on these assumptions, the power spectra of several uncorrupted and motion corrupted PPG sections were analyzed.

We observed that the power spectra of PPG sections corrupted with motion artifacts presented several random components that do not represent the fundamental characteristics of the underlying uncorrupted signal, resulting in random and significant changes in the period domain characteristics. In figure 6 it is possible to observe significant changes in the power,

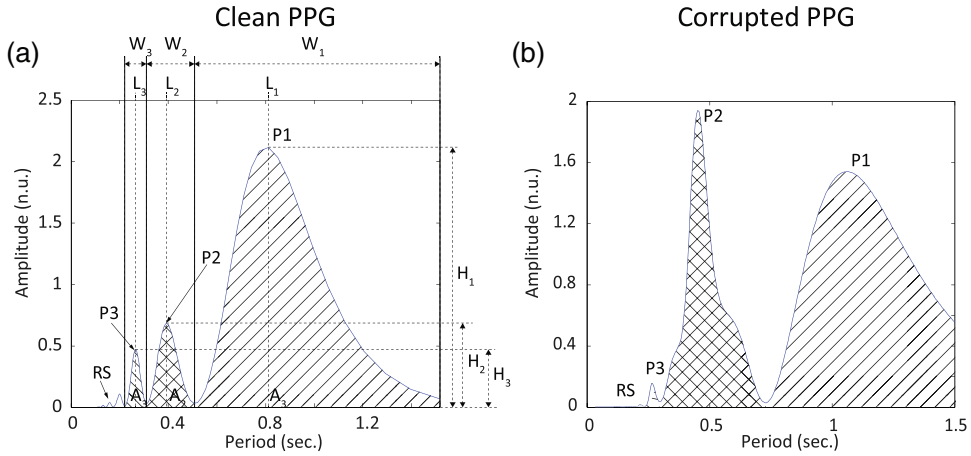

Figure 5. Representation of the PPG signal period domain spectrum, its major components (P_1, P_2 and P_3) and the remaining spectrum (RS) for: (*a*) clean and (*b*) corrupted PPG sections.

location and length of the main components of the spectra between 20 s and 42 s, where the PPG signal is corrupted by motion artifacts.

To capture these variations, the PD-STFT of each PPG section was analyzed and the following characteristics were defined (see figure 5): (1) height (H); (2) location (L); (3) width (W); and (4) area (A). These characteristics are defined as $pCh_{1,\ldots,4} : \{H, L, W, A\}$, while the three most relevant spikes and the remaining spectrum are defined as P_1, P_2, P_3 and RS. The variations of $P_{1,2,3}$ characteristics were evaluated by equation (8), resulting in the features $F_{8,\ldots,19}$, which are presented in figure 7.

$$F_{8,\ldots,19} = \Delta\left(pCh_i^{P_k}\right) = \left|pCh_i^{P_k}(j) - pCh_i^{P_k}(j-1)\right|, \text{ for } i = 1, \ldots, 4 \text{ and } k = 1, 2, 3 \tag{8}$$

where, pCh_i is the ith period characteristic, k is the spike index and j is the pulse (section) index.

Additionally, the relationship between characteristics of the two most relevant spikes (P_1 and P_2) was also assessed and was defined as follows:

$$F_{20,\ldots,23} = \Delta\left(pCh_i^{P_1} - pCh_i^{P_2}\right), \; i = 1, \ldots, 4. \tag{9}$$

An example of the rate of changes of the relationship between the two most relevant peaks characteristics, i.e. $F_{20,\ldots,23}$ are presented in figure 8.

The area $\left(pCh_4\right)$ of the *RS* and its relationship with the sum of the three most relevant peaks area was also considered:

$$F_{25} = \Delta\left(\frac{pCh_4^{RS}}{pCh_4^{P_1} + pCh_4^{P_2} + pCh_4^{P_3}}\right). \tag{10}$$

An example of the rate of change of the aforementioned characteristics, i.e., $F_{24} = \Delta\left(Ch_4^{RS}\right)$ and F_{25}, is presented in figure 9.

Assuming that the main period characteristics of the PPG signal are represented by the most relevant components in the distribution and that the remaining components are the result of noise and motion artifacts, a model of the original distribution was created based on the 3

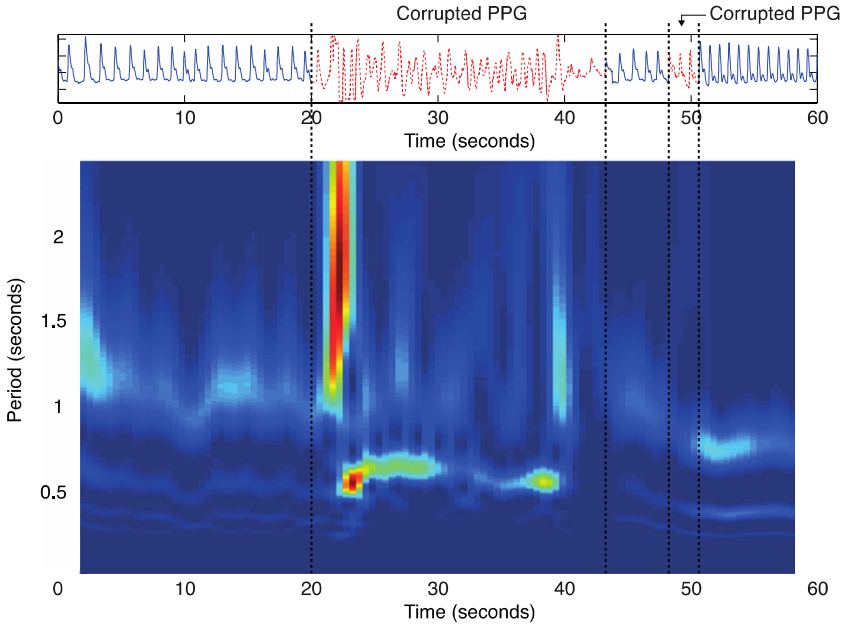

Figure 6. Period domain spectrogram of the PPG signal showing clear changes in the spectra fundamental characteristics in the presence of motion artifacts.

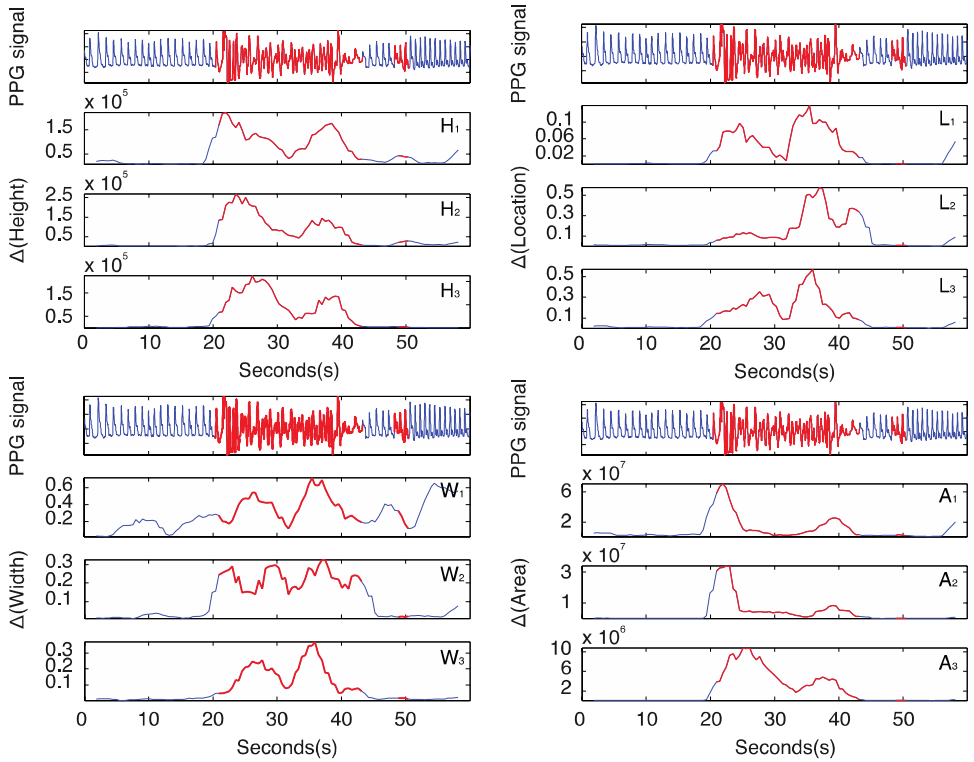

Figure 7. Rate of changes of the three most relevant spikes' characteristics (height, location, width and area).

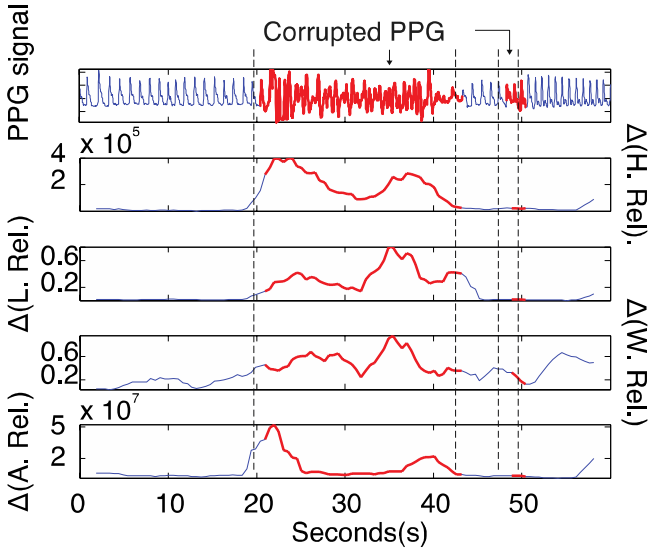

Figure 8. Rate of change of the relationship between the characteristics of the two most relevant peaks (P_1 and P_2).

most relevant spikes, using Gaussian functions. The parameters of each Gaussian are determined based on the height $\left(Ch_1^{Pi}\right)$ and location $\left(Ch_2^{Pi}\right)$ of the detected spikes $(i = 1, \ldots, 3)$. The spectrum model (X^m) was defined as:

$$\mathrm{X}^m(s) = \sum_{i=1}^{3} pCh_1^{Pi} \mathrm{e}^{-\frac{\left(s-pCh_2^{Pi}\right)^2}{2a_{Pi}^2}}, a_{Pi} = \frac{FWHM_{Pi}}{2\sqrt{2\ln 2}} \tag{11}$$

where s is the period and $FMHM_{Pi}$ is the full width at half maximum of the spike Pi and ln is the natural logarithm.

The comparison between the computed spectrum model (X^m) and the original spectrum (X^o) was then evaluated using Kullback–Leibler divergence measure (equation (12)).

$$F_{26} = D_{KL}\left(X^m; X^o\right) = \sum_s X^m(s) \ln\left(\frac{X^m(s)}{X^o(s)}\right) \tag{12}$$

where s is the period.

The rationale behind this comparison is that the increase in the spectrum's complexity, as a result of the inclusion of random components, can be detected by an increase in the Kullback–Leibler divergence between the original spectrum and the computed spectrum model (see figure 9—bottom).

2.4. Feature selection

In the feature selection step, the objective is to select a subset that contains the most relevant and least redundant features for the discrimination of motion artifacts. This enables the interpretability of the classification model to be built upstream, and improves the efficiency classification model and its generalization capability.

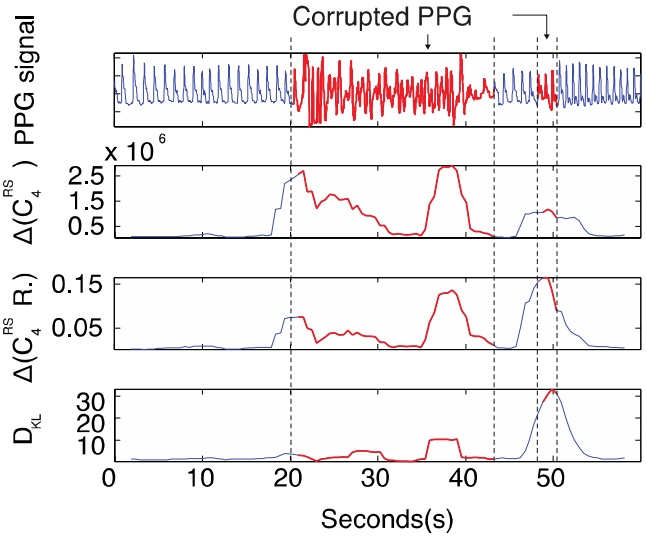

Figure 9. Rate of change of characteristics 24 and 25, and feature 26.

In this paper the feature selection process was performed using the Normalized Mutual Information Feature Selection (NMIFS) method, proposed by Estevez at al. (2009), which is an enhancement to its predecessor methods, the Battiti's MIFS (Battiti 1994), MIFS-U (Kwak and Chong-Ho 2002) and mRMR (Peng *et al* 2005). The main enhancement of the NMIFS method over its predecessors is the introduction of the Normalized Mutual Information (*nMI*) (equation (13)) as a measure of redundancy and the fact that there is no need for user defined parameters. The selection criterion used in the NMIFS method is presented in equation (14).

$$nMI\left(F_i;F_s\right)=\frac{MI\left(F_i;F_{se}\right)}{\min\left\{H\left(F_i\right),H\left(F_{se}\right)\right\}} \tag{13}$$

F_i and F_j are the features i and j of a set of features F, $MI(F_i, F_j)$ is the mutual information (MI) between features i and j and $H\left(F_{\mathrm{se}}\right)=\sum_{f_{\mathrm{se}}\in \mathrm{SE}} P\left(F_{\mathrm{se}}\right)\log P\left(F_{\mathrm{se}}\right)$ is the entropy.

$$G\triangleq \mathrm{MI}\left(\mathrm{CL};F_i\right)-\frac{1}{|\mathrm{SE}|}\sum_{F_{\mathrm{se}}\in \mathrm{SE}} nMI\left(F_i;F_{\mathrm{se}}\right) \tag{14}$$

where G is the NMIFS score, $\mathrm{SE}=\{F_{\mathrm{se}}\}$, for $\mathrm{se}=1,\ldots,|\mathrm{SE}|$ is the subset of selected features and CL is the classes variable.

2.5. Classification

A support vector machine (SVM) model has been adopted for the discrimination between motion artifacts and clean PPG. The classification process was performed using the algorithm C-support vector classification (C-SVC) algorithm (Chang and Lin 2011), with a radial basis function kernel.

Given the training vector $Tv^i\in R^n, i=1,\ldots,l$, and the correspondent classes label $Cl^i\in\{-1,1\}$, the C-SVC optimization problem requires the solution for:

Table 1. Volunteers' characteristics (average ± standard deviation).

	Healthy	CVD
Age	27.4 ± 3.7	62 ± 13.5
Weight	72.5 ± 8	87.9 ± 21.4
BMI	24.4 ± 2.9	31.5 ± 6.9
Male/female	8/0	5/2

$$\min_{w,b,\xi} \frac{1}{2} w^T w + C \sum_{i=1}^{l} \xi_i \tag{15}$$

$$\text{subject to } Cl^i (w^T \phi (Tv^i) + b) \geq 1 - \xi_i, \ \ \xi_i \geq 1. \tag{16}$$

Here, the function ϕ maps the training vectors Tv^i into a higher dimensional space, and the cost, $C>0$, is the penalty parameter for the error term. The radial basis function kernel, $K(Tv^i, Tv^j) = \phi(Tv^i)^T \phi(Tv^j)$ is defined by:

$$K(Tv^i, Tv^j) = \exp(-\gamma Tv^i - Tv^{j\,2}), \gamma>0 \tag{17}$$

where the parameter gamma (γ) is a RBF kernel specific parameter.

3. Results and discussion

3.1. Experimental protocol

To evaluate the performance of the proposed algorithm, a data collection study was conducted aiming at the collection of photoplethysmograpic (PPG) signals from 15 volunteers: 8 healthy volunteers were enrolled at the Faculty of Sciences and Technology of the Coimbra University and 7 patients with cardiovascular diseases (CVD) were enrolled at the cardiovascular department infirmary of the Hospital Center of Coimbra University. The biometric characteristics of the 15 subjects involved in the present study are summarized in table 1.

The PPG waveform was recorded from the tip of the index finger using an infrared transmission finger probe with a HP-CMS monitor and was digitized at a sampling frequency of 125 Hz.

In order to conduct a wide variety of motion artifact patterns, the subjects were asked to execute two runs of eleven different types of hand and body movements (see figure 10), resulting in 22 records of 60 s for each subject. In order to correctly and timely execute the movements, each volunteer was guided by a slideshow, which showed the expected movement pattern, the next movement and the time to the next movement. Additionally, a trained technician also assisted the volunteers during the whole process.

The volunteers were asked to perform each movement in the 20–40 s. time interval of each run. A technician annotated each record in order to identify the exact time interval where the motion artifacts occurred.

The study was authorized by the ethical committee of the Centro Hospitalar de Coimbra in 2010 under the protocol 'Assessment of cardiac function using heart sounds, ICG and PPG'.

3.2. Feature selection

The NMIFS algorithm was applied to the whole database containing the records of both healthy and CVD volunteers. From the analysis of the computed NMIFS scores, the 8 most

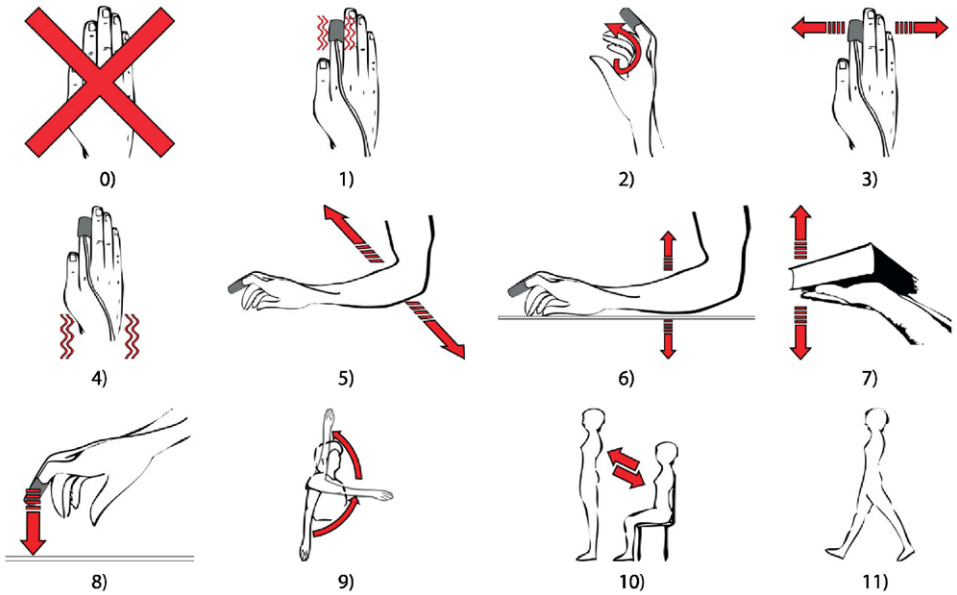

Figure 10. Movements performed by the volunteers. (0) No movement; (1) disturbance of the PPG probe, causing variations in the contact point between fingertip and probe; (2) gently bending of the index finger; (3) repeated movement of the wrist left and right; (4) shaking the wrist; (5) repeated movement of the epsilateral arm in the horizontal plane; (6) repeated movement of the epsilateral arm in the vertical plane; (7) lifting and lowering a book with both hands; (8) repeated tapping of the table with the index finger; (9) repeated raising and lowering of the arm; (10) repeated sitting down and standing up; (11) slow walking in a straight line.

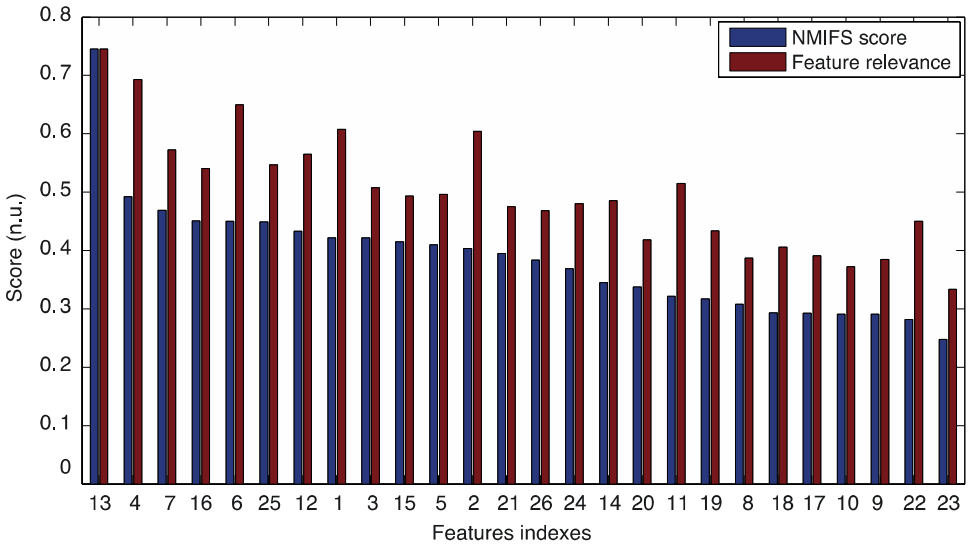

Figure 11. NMIFS and relevance scores for the 26 features extracted from the time $(F_{1,\ldots,7})$ and period $(F_{8,\ldots,26})$ domain analysis.

Table 2. Results achieved by the proposed methodology in Global, healthy and CVD subsets.

	Performance metric (avg ± std)		
Context	SE	SP	ACC
Global	84.3 ± 0.8	91.5 ± 0.5	88.5 ± 0.4
Healthy	78.4 ± 1.2	94.4 ± 0.6	87.5 ± 0.6
CVD	91 ± 0.8	88.4 ± 0.9	89.5 ± 0.6

relevant features were selected, corresponding to 4 features from the time domain and 4 features from the period domain. From the time domain, the selected features are pulse amplitude (F_1) , trough depth difference (F_4) , pulse skewness (F_6) and pulse kurtosis (F_7) . In the period domain, the location of the 2nd and 3rd major spikes (F_{12} and F_{13}), the length of the 3rd major spike (F_{16}) and relationship of the major spikes area with the remaining spectrum (F_{25}) were selected. The two most relevant selected features derive from the period domain analysis, showing its importance in the proposed methodology.

In figure 11 we present the scores achieved by the NMIFS algorithm as well as the relevance scores ($\mathrm{M}I\,(CL; F_i)$, equation (14)).

3.3. Classification

The 176 recorded signals were analyzed and each section was classified using the proposed methodology and compared to the manually annotated classification. The performance of the algorithm was evaluated for the global, healthy and CVD dataset, as well as to each of the 11 motion sources.

In order to generate a classification model that can accurately predict the testing data and to avoid the over fitting problem, it is essential to find the parameters gamma (γ) and cost (C) that best suit the present classification problem. Therefore, a grid-search method using 10-fold cross-validation was used for this proposal. The global dataset was randomly partitioned into 10 equal size subsets. From the 10 subsets, 9 subsets were used for training and the remaining subset was used for testing. The cross-validation process was repeated 10 times with each of the k subsets used exactly once as the validation data and its accuracy is the average accuracy in each testing step. The cross-validation process was repeated several times with groups of exponentially growing gamma/cost pairs ($C = 2^{-5}, 2^{-3}, \ldots, 2^{15}$ and $\gamma = 2^{-15}, 2^{-13}, \ldots, 2^{9}$). The parameters that best fit the current classification problem were defined as: $C = 2^{5.33}$ and $\gamma = 2^{6.35}$.

The validation of the proposed methodology was performed using a 10-fold cross-validation scheme. In this process, the global dataset was randomly partitioned into 10 equally sized subsets with the same percentage of samples from each patient and each motion artifact source. Nine subsets were used for training the classification model, while the remaining subset was used for validation. The data of the validation subset corresponding to each context was used to validate the classification model regarding each subject group and motion artifacts' source. This process was repeated for each of the 10 subsets. The 10-fold cross validation procedure was conducted 20 times. The performance of the proposed methodology was defined by the average ± standard deviation (over the 20 repetitions) of the following metrics: sensitivity (SE) and specificity (SP), and accuracy (ACC).

Table 2 summaries our results. The proposed methodology achieved a good performance in the classification of both corrupted and clean PPG sections, with an overall accuracy of 88.5%, which corresponds to a sensitivity of 84.3% and a specificity of 91.5% during

Table 3. Comparison of the results achieved by the proposed method and the methods proposed in the literature (Sukor *et al* 2011, Krishnan *et al* 2008) in healthy volunteers.

	Performance metric (avg ± std)		
Healthy	SE	SP	ACC
Proposed method	78.4 ± 1.2	94.4 ± 0.6	87.5 ± 0.6
Sukor *et al* (2011)	89 ± 10	77 ± 19	83 ± 11
Krishnan *et al* (2008)	91/97	94/80	n.d.

Table 4. Results achieved by the proposed methodology for each of the 11 motion artifacts' sources.

	Performance metric (avg ± std)		
Context	SE	SP	ACC
Movement 1	84.7 ± 3	92.6 ± 1.6	89.7 ± 1.5
Movement 2	90 ± 1.9	91.7 ± 1.8	91 ± 1.3
Movement 3	72.7 ± 3	93.5 ± 1.4	85.1 ± 1.3
Movement 4	83.9 ± 2.6	92.7 ± 1.7	89.3 ± 1.5
Movement 5	81.6 ± 2.9	91.9 ± 1.7	87.9 ± 1.6
Movement 6	85.5 ± 2.6	91.5 ± 1.5	89 ± 1.5
Movement 7	88.1 ± 2.4	90.6 ± 1.9	89.4 ± 1.5
Movement 8	77.5 ± 2.7	89.8 ± 1.9	84.6 ± 1.6
Movement 9	89.6 ± 2	92.2 ± 1.7	91 ± 1.2
Movement 10	87.6 ± 2.1	89.3 ± 1.8	88.5 ± 1.4
Movement 11	83.9 ± 2.4	90.9 ± 2.1	88 ± 1.5

validation. Looking into more detail in the specific subject groups, for healthy subjects the accuracy decreased to 87.5%, whereas for the CVD patients an increase can be observed to 89.5%. However, while in the CVD dataset the proposed methodology is able to discriminate corrupted PPG sections from the clean ones with high sensitivity (91.0%) and specificity (88.4%), in the healthy dataset, there is a significant decrease in sensitivity (78.4%). These results show that the proposed methodology is able to detect motion artifacts more accurately in CVD volunteers when compared to healthy volunteers. One possible reason for this difference in the presented results relies on the different characteristics of the PPG signal within healthy and CVD subjects. Due to ageing and the appearance of cardiovascular complications, the compliance of the systemic vascular wall decreases (i.e. arterial stiffening), leading to the disappearance of the dicrotic notch and therefore changing the morphological complexity of the PPG waveform in the CVD volunteers. Additionally, the appearance of abnormal cardiovascular events (e.g. arrhythmias) in CVD volunteers also affects the period characteristics of the PPG waveform, leading to the misclassification of clean PPG sections and reducing the model specificity in the subject group. Since the extracted features mainly reflect the changes in these characteristics, it is expectable to have variations in the extracted features discrimination capability and therefore different optimal feature space for healthy and CVD subsets. The presented results suggest that the discrimination capability of the selected features is dependent on the analyzed context, i.e. the analyzed volunteer subset, affecting the proposed methodology performance within healthy and CVD subjects, as shown in table 2.

It is not possible to perform a fair comparison between the proposed algorithm and state of the art, since different datasets were adopted, resorting on dissimilar populations and protocols. However, a comparison of algorithms performance within the Healthy

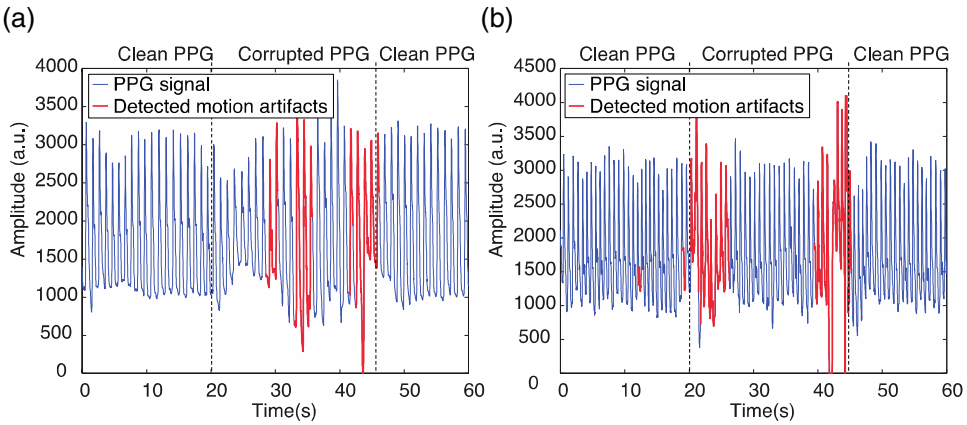

Figure 12. Examples of PPG signals when a performance decrease in the proposed methodology was observed. (*a*) Volunteer 4/Record 5/Movement 3. (*b*) Volunteer 3/Run 15/Movement 8.

population can still be done. From table 3 we present a comparison of the results achieved by the current algorithm with the methods presented in literature. On the one hand, it is possible to observe that the specificity and accuracy of the current algorithm are greater (SP: +17.4% and ACC: +4.5%) compared to the algorithm presented by Sukor *et al* (2011). Contrarily, the sensitivity of the current algorithm remains lower than the later method (SE: −10.6%). Nonetheless, the algorithm proposed in (Sukor *et al* 2011) exhibits a excessive uncertainty in the results, revealed by the high standard deviation (from 10% to 19%) of the used metrics. On the other hand, one can observe that the current algorithm was not able to outperform the one proposed by Krishnan *et al* (2008), with a much lower sensitivity (SE: −12.6%) and a marginally higher specificity (SP: +0.4). The author did not report the accuracy of the proposed algorithm and therefore we were not able to compare both algorithms using this metric.

From table 4 it can be observed that the majority of the movement artifacts are identified with accuracy over 88%. However, there are two exceptions for the 3rd and 8th movement artifacts where a decrease in the detection accuracy has been observed (85.1% and 84.6%, respectively). This is a result of an evident increase of the algorithm's inability to detect properly the corrupted PPG sections, shown by the decrease in sensitivity to 72.7 and 77.5%, respectively. On the other hand, the algorithm's specificity, that is, the ability to detect non-corrupted PPG sections is still high.

The performance decrease for the 3rd and 8th movement artifacts is possibly associated with how the volunteers perform the requested movements. Two possible reasons are the: i) Low corruption of PPG data resultant from the incorrect execution of the performed movement and; ii) Increase in the periodicity of the performed movements.

During the execution of the 3rd movement, (see figure 10) several volunteers gently lifted the wrist/probe, causing no friction between the PPG probe and wrist with the table, and therefore resulting in low corruption of PPG data. Additionally, during the execution of movement 8, it was observed that several volunteers performed this task in a periodic fashion (contrarily to what is expected in real scenarios), leading to contamination of the PPG data with periodic artifacts. Since the present methodology is based on the analysis of the changes in the period components of the PPG data, artifacts with an intrinsic periodicity typically cannot be

detected. In figure 12, we present two examples where the aforementioned problems occurred and consequently a decrease the proposed algorithm performance has been observed.

4. Conclusion

In the current paper a novel methodology for the detection of motion artifacts in photoplethysmographic signals has been proposed. Our approach is based on the analysis of the time and period domain analysis of the PPG leading to the extraction of a total of 26 features. Contrarily to clean PPG signals, were changes on the PPG pulse morphology are mainly caused by cardiovascular changes, corrupted PPG signals show abnormal, erratic and 'random' pulse characteristics. To assess these, the morphology of the PPG pulses and their relationships with neighboring pulses was analyzed contributing to the extraction of eight time domain 8 features. Features extracted from the period domain resorts on the principle that, the PD-STFT also exhibits a regular shape representing the main features of the signal similar to the morphology of the PPG signal. From the period spectra analysis, it was found that a clean PPG signal consists of three major spikes with different locations, lengths and amplitudes, being the most relevant spike a result of the fundamental period of the PPG signal, and the remaining spikes associated to location and amplitude of the waves reflected from the periphery towards the aorta. Moreover one observed that in corrupted sections of the PPG signal, several random components that do not represent the fundamental characteristics of the underlying uncorrupted signal in the presence of motion artifacts are present, leading to random and significant changes in the period domain characteristics. To capture these changes, 18 features were extracted from the analysis of the main characteristics of the period domain spectra of the PPG signal.

In order increase the classification model generalization capability and interpretability, the extracted features were ranked using the NMIFS algorithm and the 8 most relevant features were selected, corresponding to 4 features from the time domain (pulse amplitude, trough depth difference, pulse skewness and pulse kurtosis) and 4 features from the period domain (2nd and 3rd major spikes, the length of the 3rd major spike and relationship of the major spikes area with the area remaining spectrum).

The discrimination between motion artifacts and clean PPG sections was performed using C-Support Vector Classification algorithm (Chang and Lin 2011), with a radial basis function kernel. The identification of the most suitable gamma (γ) and cost (C) parameters was performed using a 10-fold cross-validation grid-search method.

The proposed methodology for motion artifacts' detection was validated on 8 healthy volunteers enrolled a the Faculty of Sciences and Technology of the Coimbra University and 7 CVD patients enrolled at the cardiovascular department infirmary of the Hospital Center of Coimbra University. A 10-fold cross-validation scheme was repeated 20 times with the following performance metrics: sensitivity (SE), specificity (SP), and accuracy (ACC).

The results achieved by the current algorithm in the global dataset (SE: 84.3% and SP: 91.5%) suggest that the characteristics of period components of the PPG signal can be used as discriminative features for motion artifact detection. Additionally, the results achieve for each of the volunteers subsets, show that the proposed methodology is able to detect motion artifacts more accurately in CVD volunteers (SE: 91% and SP: 88.4%) when compared to healthy volunteers (SE: 78.4% SP: 94.4%), suggesting a different discrimination capability of both time and period domain features for each of the volunteers subsets. Finally, the results achieved for each of the motion artifact sources show that the proposed methodology is able to detect motion artifacts with high accuracy regardless the performed movement.

Acknowledgments

The authors would like to express their gratitude for the support of 'Centro Hospitalar de Coimbra' and specially the effort of Dr Leitão Marques in facilitating the arrangements for the data acquisition component of the present study.

This work was supported by CISUC (Center for Informatics and Systems of University of Coimbra) and by EU projects HeartCycle (FP7-216695), iCIS (CENTRO-07-ST24-FEDER-002003).

Declaration of interest

Jens Muehlsteff is employed by Philips Research in the Netherlands.

References

Abramowitz M and Stegun I A 2012 *Handbook of Mathematical Functions: with Formulas, Graphs, and Mathematical Tables* (New York: Dover)

Addison P *et al* 2012 Developing an algorithm for pulse oximetry derived respiratory rate (RRoxi): a healthy volunteer study *J. Clin. Monit. Comput.* **26** 45–51

Allen J 2007 Photoplethysmography and its application in clinical physiological measurement *Physiol. Meas.* **28** R1

Baruch M *et al* 2011 Pulse decomposition analysis of the digital arterial pulse during hemorrhage simulation *Nonlinear Biomed. Phys.* **5** 1

Battiti R 1994 Using mutual information for selecting features in supervised neural net learning *Trans. Neur. Netw.* **5** 537–50

Chan G H *et al* 2007 Automatic detection of left ventricular ejection time from a finger photoplethysmographic pulse oximetry waveform: comparison with Doppler aortic measurement *Physiol. Meas*, **28** 439

Chang C-C and Lin C-J 2011 LIBSVM: a library for support vector machines *ACM Trans. Intell. Syst. Technol.* **2** 27:1–27

Cook L B 2001 Extracting arterial flow waveforms from pulse oximeter waveforms *Anaesthesia* **56** 551–5

Dawber T R, Thomas H E and McNamara P M 1973 Characteristics of the dicrotic notch of the arterial pulse wave in coronary heart disease *Angiology* **24** 244–5

Estevez P A *et al* 2009 Normalized mutual information feature selection *Neural Netw IEEE Trans* **20** 189–201

Foo J Y A 2006 Comparison of wavelet transformation and adaptive filtering in restoring artefact-induced time-related measurement *Biomed. Signal Process. Control.* **1** 93–8

Foo J and Wilson S 2006 A computational system to optimise noise rejection in photoplethysmography signals during motion or poor perfusion states *Med. Biol. Eng. Comput.* **44** 140–5

Gibbs P and Asada H H 2005 Reducing motion artifact in wearable bio-sensors using MEMS accelerometers for active noise cancellation *Conf. Proc. of the American Control Conf, 2005.* IEEE, 2005.

Graybeal J M and Petterson M T 2004 Adaptive filtering and alternative calculations revolutionizes pulse oximetry sensitivity and specificity during motion and low perfusion *IEMBS '04. 26th Annual Int Conf of the IEEE* (*San Francisco, California, USA*) (Engineering in Medicine and Biology Society)

Han H, Kim M J and Kim J 2007 Development of real-time motion artifact reduction algorithm for a wearable photoplethysmography *Conf. Proc. IEEE Eng. Med. Biol. Soc.* **2007** 1538–41

Kim B S and Yoo S K 2006 Motion artifact reduction in photoplethysmography using independent component analysis *Biomed. Eng. IEEE Trans* **53** 566–8

Kim S H, Ryoo D W and Bae C 2007 Adaptive noise cancellation using accelerometers for the PPG signal from forehead *Conf. Proc. IEEE Eng. Med. Biol. Soc*. **2007** 2564–7

Krishnan R, Natarajan B and Warren S 2008 Analysis and detection of motion artifact in photoplethysmographic data using higher order statistics *IEEE Int. Conf. on ICASSP (Las Vegas, California, USA, 2008) Acoustics, Speech and Signal Processing*

Kunchon S, Desudchit T and Chinrungrueng C 2009 Comparative evaluation of adaptive filters in motion artifact cancellation for pulse oximetry *5th Int Colloquium on CSPA 2009* (*Kuala Lumpur, Malaysia, 2004*) Signal Processing & its Applications

Kwak N and Chong-Ho C 2002 Input feature selection for classification problems *Neural Netw. IEEE Trans.* **13** 143–59

Lee C M and Zhang Y T 2003 Reduction of motion artifacts from photoplethysmographic recordings using a wavelet denoising approach *IEEE EMBS Asian-Pacific Conf. on Biomedical Engineering* (*Kyoto-Osaka-Nara, Japan, 2003*)

Lee J *et al* 2004 Design of filter to reject motion artifact of pulse oximetry *Comput. Stand. Interfaces* **26** 241–9

Peng H, Fulmi L and Ding C 2005 Feature selection based on mutual information criteria of max-dependency, max-relevance, and min-redundancy *Pattern Anal. Mach. Intell. IEEE Trans.* **27** 1226–38

Raghuram M *et al* 2012 A novel approach for motion artifact reduction in PPG signals based on AS-LMS adaptive filter *IEEE Trans. Instrum. Meas.* **61** 1445–57

Reddy K A and Kumar V J 2007 Motion artifact reduction in photoplethysmographic signals using singular value decomposition *Instrumentation and Measurement Technology Conf. Proc.* (*Warsaw, Poland, 2007*) (IMTC)

Reddy K A, George B, Kumar V J 2008 Motion artifact reduction and data compression of photoplethysmographic signals utilizing cycle by cycle fourier series analysis *Instrumentation and Measurement Technology Conf. Proc.* (*IMTC*) (IEEE)

Reisner A *et al* 2008 Utility of the photoplethysmogram in circulatory monitoring *Anesthesiology* **108** 950–8

Shang A B *et al* 2007 Development of a standardized method for motion testing in pulse oximeters *Anesth. Analg.* **105** S66–77

Sukor J A, Redmond S J and Lovell N H 2011 Signal quality measures for pulse oximetry through waveform morphology analysis *Physiol. Meas*. **32** 369

Sun Y, Chan K and Krishnan S 2005 Characteristic wave detection in ECG signal using morphological transform *BMC Cardiovasc. Disord* **5** 28

Wisely N A and Cook L B 2001 Arterial flow waveforms from pulse oximetry compared with measured Doppler flow waveforms *Anaesthesia* **56** 556–61

Wood L B and Asada H 2007 Low variance adaptive filter for cancelling motion artifact in wearable photoplethysmogram sensor signals *Conf. Proc. IEEE Eng. Med. Biol. Soc.* **2007** 652–5

Yan Y-S, Poon C and Zhang Y-T 2005 Reduction of motion artifact in pulse oximetry by smoothed pseudo Wigner-Ville distribution *J. NeuroEng. Rehabil.* **2** 3

Yousefi R, xNourani C and Panahi I 2012 Adaptive cancellation of motion artifact in wearable biosensors *Engineering in Medicine and Biology Society (EMBC) Annual Int. Conf. IEEE* (San Diego, CA: IEEE)